# THIN FILM PIN PHOTODIODES FOR OPTOELECTRONIC SILICON ON SAPPHIRE CMOS

*A. Apsel*

Cornell University
Ithaca, NY, 14853

*E. Culurciello, A. G. Andreou, K. Aliberti*

Johns Hopkins University
Baltimore, MD, 21218

## ABSTRACT

In this paper, we consider both the utility of SOS substrates as a vehicle for optoelectronic packaging and the high speed silicon photodiodes available on a commercial SOS process. We show optical responses for six configurations of PIN photodiodes designed in this process. Our results indicate that photodiodes native to this process will operate at better than gigabit rates and produce signals over a range of visible wavelengths.

## 1. INTRODUCTION

Silicon on Insulator (SOI) CMOS technology is an emergent technology, poised to replace bulk CMOS for deep sub-micron VLSI [1]. The strength of traditional SOI as a candidate technology comes purely from its electrical properties. Devices produced in SOI are electrically isolated from one another, reducing parasitic capacitances, eliminating latch-up paths, and decreasing cross-talk. As a result, the delay and power consumption of these circuits can have up to a 300 percent performance gain over bulk CMOS circuitry [2].

Silicon on Sapphire (SOS) CMOS is a subset of SOI technology. It has long been considered a low performance alternative to standard SOI due to poor lattice matching of epitaxially grown silicon on sapphire. Recent developments in production of SOS CMOS using strained silicon have virtually eliminated these problems. Peregrine's ultra-thin silicon on sapphire (UTSi$^{TM}$) CMOS process now produces low leakage currents and $f_{max}$s in excess of 50 GHz for a .5$\mu$m process.

Unlike oxide based SOI CMOS technology, SOS CMOS offers advantages beyond its electrical properties. In addition to its usefulness as a high speed, low power CMOS platform, SOS wafers have desirable optical properties. In this paper we discuss the characteristics of sapphire substrates and thin film PIN photodiodes fabricated in a 0.5 $\mu$m SOS process. This technology is unique in that the sapphire substrate is transparent to wavelengths that may be absorbed by native photodetectors. While optical transmission through bulk substrates of 1330nm and 1550nm light has been demonstrated [3], native detectors cannot be utilized in these bulk CMOS or conventional oxide based SOI routing schemes as they can in SOS systems. We contend that thin film SOS photodiodes along with the characteristics of sapphire substrates allow the construction of opto-electronic systems with high-speed native photodetectors.

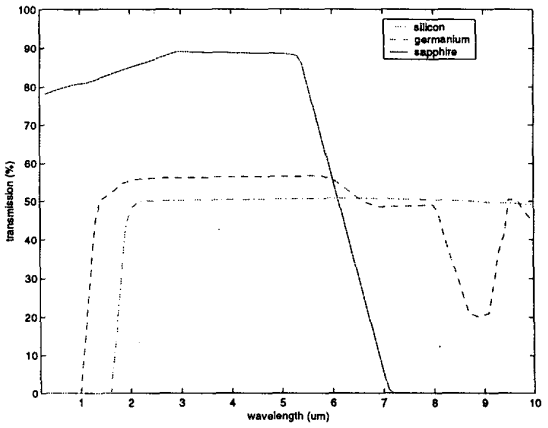


Figure 1: Transmission curves for sapphire, silicon, and germanium. [4]

## 2. OPTICAL PROPERTIES OF SAPPHIRE SUBSTRATES

Packaging of optoelectronic VLSI systems can be greatly simplified when signals transmit directly through electronic substrates [5, 3]. This also simplifies flip bonding of any front side contact optical elements such as VCSEL's or passive nano-photonics. Unfortunately, standard bulk and SOI CMOS wafers do not have good optical properties for our purposes, as shown in figure 1. The data indicates that over the wavelengths of commercially available VCSEL sources (850nm, 980nm) both silicon and germanium are opaque. Even in upper wavelength ranges of 1550nm, transmission in silicon is well below 100 percent and development of through wafer interconnects requires significant thinning of the substrate. Working systems have been produced at 1310nm and 1550nm using this technique, [3], however the complexity of this approach as well as the optical loss incurred adds cost and reduces yield significantly. Furthermore, working systems have not been constructed which include native photodetectors, crucial to high speed monolithic receiver design.

As opposed to bulk CMOS and SiGe wafers, SOS wafers allow through substrate transmission of optical signals from 300nm up to 6$\mu$m as shown in figure 1. We see that the transmission through sapphire is typically better than 80 percent over this wavelength range, reducing the need for thinned substrates when compared to bulk CMOS wafers. While internal reflections at interfaces of silicon nitride, silicon dioxide and sapphire do create addi-

0-7803-7761-3/03/$17.00 ©2003 IEEE

tional losses if post-processing is not performed, these losses will account for no more than a 12 percent loss of the transmitted light in the 400nm to 6$\mu$m wavelength range. We also note that SOS wafers combine two materials, silicon and sapphire that allow both transmission and absorption over a range of wavelengths.

## 3. NATIVE PHOTODIODES

In this section we present the characteristics of PIN photodiodes constructed in a commercial silicon on sapphire process. All of the photodiodes tested were fabricated in the Peregrine .5 $\mu$m UTSi$^{TM}$ SOS process. The silicon layer in this process is epitaxially grown on a sapphire substrate and oxidized down to a thickness of 100nm. We present the results of tests performed on six PIN photodiodes of various geometries. We constructed all devices from abutting regions of low threshold "intrinsic" n and p silicon. We blocked the source drain implant doping in the junction region. The width of the source/drain block varies for different device geometries.

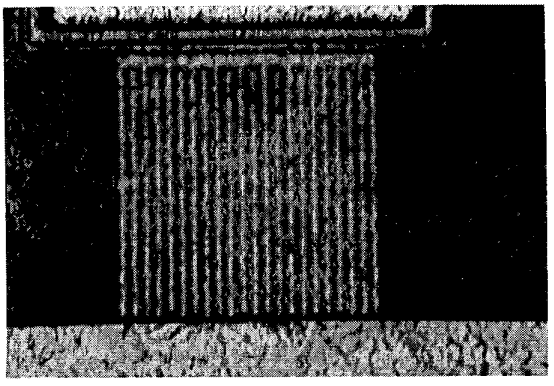

Figure 2: SOS PIN photodiode with interdigitated fingers.

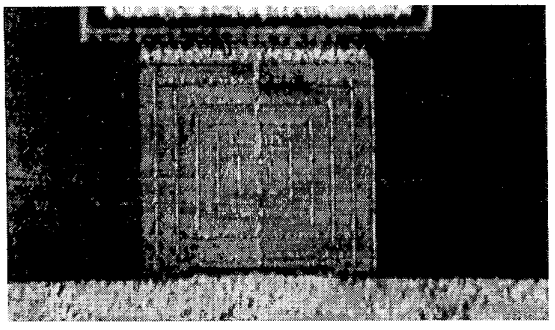

Figure 3: SOS PIN photodiode with concentric ring.

We tested six devices of two geometries shown in figures 2 and 3. All devices are in either a parallel finger PIN photodiode geometry as in figure 2 or in a ring geometry as shown in figure 3. Three devices are 65$\mu$m×65$\mu$m in size. Of these there is one ring photodiode with metal contacts to the source/drain implanted regions, one finger photodiode with metal contacts to the source/drain implanted regions, and one finger photodiode with metal contacts placed only at the edges of the device. The other three devices are 40$\mu$m×40$\mu$m rings with variations in the lengths of designated junction regions where source/drain implants are blocked. The source/drain implant blocks are 2$\mu$m, 3$\mu$m, and 4.5$\mu$m respectively. Since these three devices have metal contacts to their source/drain implanted regions, the width of the blocked regions effects the spacing of metal contacts.

### 3.1. Spectral Response

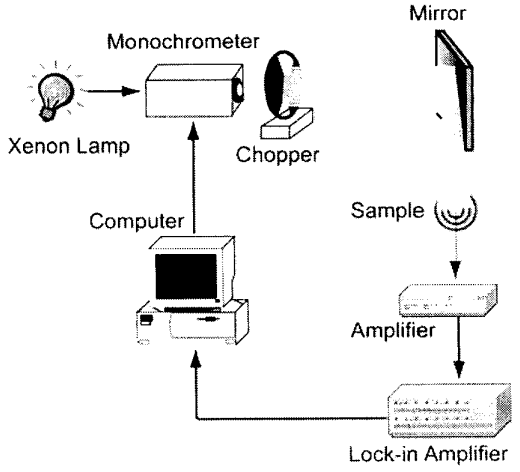


Figure 4: Experimental setup used to measure the spectral response of photo-diodes.

We measured the spectral response of the 6 geometries of thin film silicon PIN photodiodes using a Xenon lamp and the experimental set-up shown in figure 4. We measured the sensitivity of these geometries from 350nm to 850nm wavelengths with a reverse bias of 2.5V.

The resulting spectral response curves are shown in figure 5. These curves show the relative sensitivity of all photodiodes as a function of wavelength. There are several notable characteristics that are revealed in this data. We are not surprised to see that the shape of all 6 responses is very similar given that the material and the material thickness is the same in all cases. As a result the absorption of each photodiode should be similar. It is also not surprising to find that the most responsive photodiode is the device described above constructed from interdigitated fingers of p-type and n-type silicon with metal contacts only at the ends of the photodiode and not on each finger. We expect that since this device has the most open active area that it should respond most to incident light.

Next we examine the spectral response of two photodiode geometries covering the same total area. Both diodes, one ring configuration and one constructed of interdigitated fingers are 65$\mu$m×65$\mu$m and have metal contacts to p and n silicon throughout the diode but distant from the junctions. Figure 5 indicates that the response of the ring photo-diode of the same size with the same active area between contacts of 1.2$\mu$m as the finger photo-diode, has higher responsivity over the wavelength range.

Finally, we examine the response of the three 40$\mu$m×40$\mu$m ring photodiodes. The lengths of the active regions of these photodiodes are larger than the minimum 1.2$\mu$m width at 2$\mu$m, 3$\mu$m,

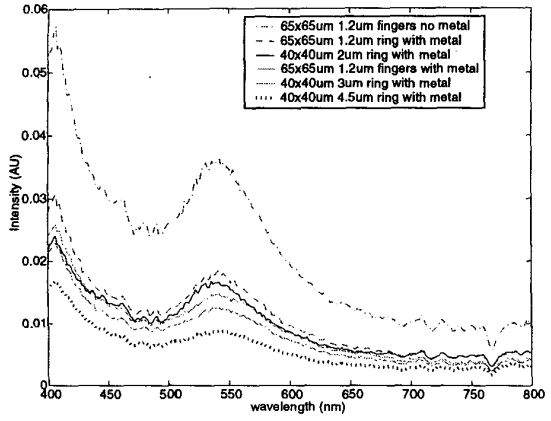


Figure 5: Spectral response of 6 geometries of thin film photodiodes in an SOS process.

and 4.5$\mu$ respectively. The intensity vs. wavelength curve indicates that the response of the photo-diodes drops with an increase in the length of the active region. We can conclude from this plot that the optimum width of an active region is below 2$\mu$m for photodiodes in this process. It is relatively simple to calculate a theoret-

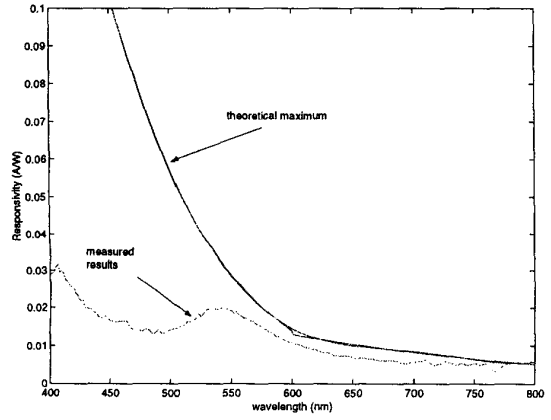


Figure 6: Responsivity of a 65×65$\mu$m thin film SOS photodiode with minimum width 1.2$\mu$m junction vs. theoretical responsivity.

ical bound on the performance of PIN photodiodes in this process. We compare the measured responsivity of the most responsive photo-diode measure to this theoretical bound. From a series of sensitivity measurements using a source of known power output, we find that 1V on the intensity curve corresponds to .27 A/W of responsivity. We normalize this to the active area of the photodiode to determine the actual responsivity of this photo-diode, shown in figure 6.

We begin calculating the maximum theoretical responsivity of PIN detectors in this process by calculating the theoretical maximum quantum efficiency, $\eta$, of a thin film of silicon. The following equation gives the quantum efficiency for a film of thickness $L$, given a surface reflectivity of $r$, and absorption as a function of wavelength for silicon, $\alpha(\lambda)$, that can be easily found in most optics texts. $\zeta$ is a fraction reflecting the percentage of electron hole pairs that contribute to photo-current.

$$\eta = (1-r)\zeta[1-e^{-\alpha L}] \tag{1}$$

$\zeta$ is a function of the quality of material used for the photodiode. For most commercial processes material is very good and this can be assumed to be unity.

Using this equation and the knowledge that L=100nm we can find a function for $\eta$ by calculating $r$ and using the absorption curve for silicon. In the peregrine UTSi$^{TM}$ process, there are a series of three interfaces through which light must be transmitted before it is incident upon the silicon sample. The first interface is from air (n=1.03) to silicon nitride (n=2). The second is from nitride to silicon dioxide (n=1.45). The third interface is between silicon dioxide and silicon (n=3.38). We can determine the total transmission to the silicon sample by assuming that reflections from back surfaces have negligible retransmission and using the following transmission equation.

$$(1-r) = T = \frac{2n_1 n_2}{(n_1+n_2)^2} \tag{2}$$

The total transmission of 0.75 is the product of the three individual surface transmissions, equal to $1-r$. This gives us a complete expression for quantum efficiency as a function of wavelength. However, we want to examine the responsivity, not quantum efficiency in our comparison. Since responsivity is the current output for a given optical power input, we use the power of incident photons as a function of wavelength to determine the theoretical responsivity as follows.

$$R = \frac{\eta q}{h\nu} = \eta\frac{\lambda(\mu m)}{1.24} = \frac{0.75\lambda}{1.24}[1-e^{-\alpha L}] \tag{3}$$

Figure 6 shows the measured responsivity of the interdigitated finger PIN photo-diode compared to the calculated maximum responsivity of a thin film silicon PIN detector. We can see from this figure that the shape of the measured and theoretical responsivity match well from 570nm to 800nm wavelengths. Below 570nm there is a dip in the responsivity of the measured curve at approximately 490nm. This dip relates to an absorption phenomena at this wavelength. This may be due to a half wave reflectance set up by a 240nm oxide layer in the layers covering the silicon. Etching and removal of these reflective layers on the native SOS photodiodes will certainly improve the responsivity of these photodiodes and perhaps bring them to the theoretical response limit.

### 3.2. Frequency Response

In addition to the spectral response discussed in the previous section, we also measured the frequency response of the aforementioned six photodetectors. We probed the samples with 40 GHz 100 $\mu$m pitch ground-signal-ground probes, focused the 785nm beam onto the sample, modulated the beam with a signal generator, and measured the output of the photodiode with a spectrum analyzer. The bias across the photodiodes is 2.5V in all cases. Figures 7 and 8 show the resulting frequency responses for the photodiodes. All responses are compensated for the bandwidth of the laser diode and normalized to show the measured bandwidth of the devices, denoted by a 3dB drop in response.

For an intrinsic region of silicon less than 5$\mu$m wide the transit time of carriers limits the speed of our detectors at approximately

10 GHz. Below this the bandwidth is limited by the resistance and capacitance of the detector itself and the circuit configuration of the experimental set-up. Figure 7 shows the frequency response

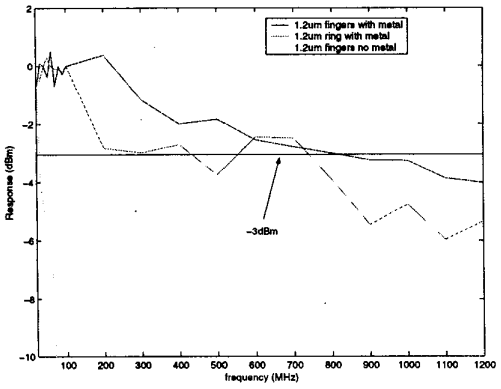


Figure 7: Frequency response of different geometries of $65\times65\mu$m SOS photodiodes.

for the three $65\mu$m$\times65\mu$m photodiodes. When we examined the spectral response of these above we noted that the most responsive device was the device which had metal contacts only on it's edges. While the responsivity of this device was nearly twice that of the equally sized devices with metal contacts, we note that the increased responsivity of this device comes with a dramatically reduced bandwidth due to increased resistance. The 3dB drop in frequency response occurs below 25 MHz, while the same geometry device with metal contacts throughout has a 3dB drop at approximately 850 MHz. The ring device has a somewhat reduced bandwidth over this geometry with a 3dB drop at approximately 450 MHz. These speeds are achievable with approximately half of the responsivity of the device without metal, making them more desirable for high speed designs where sensitivity can often be increased with only a linear reduction in bandwidth.

We note that these bandwidths are slower than expected for our junction widths. Transit times are limited to 10GHz for silicon PIN diodes less than $5\mu$m wide. Considering the lack of substrate capacitance we approximate junction capacitances for these geometries to be much less than 100pF. If we calculate resistances for the two finger geometry devices with and without metal fingers, we find device resistances of approximately 4 $\Omega$ and 7 k$\Omega$ respectively. In the case of the 4 $\Omega$ detector, the 50 $\Omega$ input capacitance of the spectrum analyzer will dominate the intrinsic resistance of this device in measurement. When we consider the cases of these two detectors, we find that the measured bandwidths indicate a capacitance between 2pF and 3pF in both devices. This is clearly not a reasonable result for $65\mu$m$\times65\mu$m thin film silicon photo-detectors. We conclude that this capacitance must be induced by the experimental set-up. If we calculate the capacitance of the 40A-100-C GSG GGB picoprobes, we find that the total capacitance to ground of these probes is approximately 2.3pF. We attribute the bandwidth limitation of these measurements to this parasitic capacitance. More accurate and aggressive photodiode bandwidths can be measured by the addition of an output buffer or amplifier stage with a small gate load on these photodiodes. These measurements still provide useful information about the photodiodes. We note that the ring configuration must be more resistive

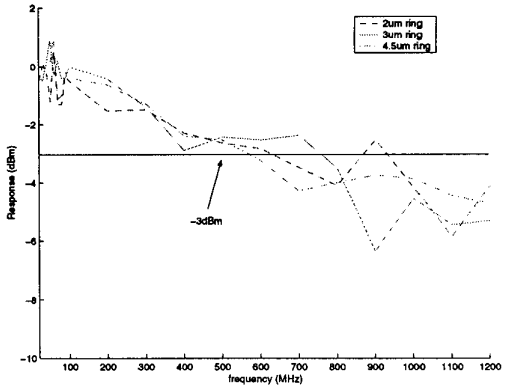


Figure 8: Frequency response of $40\times40\mu$m SOS ring photodiodes with varying junction widths.

than the finger configuration, for instance, and we see by our measured bandwidths that we can easily achieve GHz signaling rates with $65\mu$m$\times65\mu$m devices by limiting the load capacitance on the output node (now 2.3pF of probe capacitance) below 1.5pF.

While these speeds seem slow in comparison to GaAs and other direct bandgap detectors, they are fast compared to most commercial silicon PIN detectors. Honeywell's highest speed PIN detectors, for instance, have minimum rise times of 5ns under normal bias conditions. Furthermore, the SOS detectors are monolithic in a CMOS process, allowing easy integration of detectors and receiver circuitry for inexpensive packaging of opto-electronic systems at gigabit rates.

The next set of devices we tested were $40\mu$m$\times40\mu$m ring devices described in the previous section. Since the variation in these devices is the length of the region around the junction which does not have a highly doped source/drain implantation, the distance between metal contact rings is also varied. We expect that this varies the capacitance across the diode somewhat and would change the frequency response of these devices, favoring more distant contacts. However the results shown in figure 8 indicate no conclusive evidence of this due to RC bandwidth limitations of our set-up.

## 4. REFERENCES


[1] J. B. Kuo and Ker-Wei Su, CMOS VLSI *Engineering Silicon-on-Insulator*, Kluwer Accademic Publishers, 2000.

[2] S. Cristoloveanu, "SOI a metamorphosis of silicon," *IEEE Circuits and Devices*, vol. 15, no. 1, pp. 26–32, 1999.

[3] O. Vendier, S. Bond, M. Lee, S. Jung, M. Brooke, N. M. Jokerst, and R. P. Leavitt, "Stacked si CMOS circuits with a 40-Mb/s through-silicon optical interconnect," *IEEE Photonics Technology Letters*, vol. 10, no. 4, pp. 606–608, Apr. 1998.

[4] J. Jamieson, R. McFee, G. Plass, R. Grube, and R. Richards, *Infrared Physics and Engineering*, McGraw-Hill, 1963.

[5] A. Andreou, Z. Kalayjian, A. Apsel, P. O. Pouliquen, R. A. Athale, G. Simonis, and R. Reedy, "Hybrid integration of surface emitting vcsel's with ultra-thin silicon on sapphire (sos) cmos vlsi circuits," *Circuits and Systems Magazine*, Aug. 2001.